Supporting information for

Nanocrystals of Cesium Lead Halide Perovskites ($CsPbX_3$, X=Cl, Br, and I): Novel Optoelectronic Materials showing Bright Emission with Wide Color Gamut

by Loredana Protesescu,[†,‡] Sergii Yakunin, [†,‡] Maryna I. Bodnarchuk, [†,‡] Franziska Krieg,[†,‡] Riccarda Caputo,[†] Christopher H. Hendon,[§] Ruo Xi Yang,[§] Aron Walsh[§] and Maksym V. Kovalenko[†,‡]*

[†] Institute of Inorganic Chemistry, Department of Chemistry and Applied Biosciences, ETH Zürich, Vladimir Prelog Weg 10, CH-8093 Zürich, Switzerland

[‡] Laboratory for Thin Films and Photovoltaics, Empa – Swiss Federal Laboratories for Materials Science and Technology, Überlandstrasse 129, CH-8600 Dübendorf, Switzerland

[§] Centre for Sustainable Chemical Technologies and Department of Chemistry, University of Bath, Bath BA2 7AY, United Kingdom

Synthesis Methods

Preparation of Cs-oleate: Cs_2CO_3 (0.814g, Aldrich, 99.9%) was loaded into 100 mL 3-neck flask along with octadecene (40mL, Sigma-Aldrich, 90%) and oleic acid (2.5 mL, OA, Sigma-Aldrich, 90%), dried for 1h at 120 ºC, and then heated under N_2 to 150 ºC until all Cs_2CO_3 reacted with OA. Since Cs-oleate precipitates out of ODE at room-temperature, it has to be pre-heated to 100 ºC before injection.

Synthesis of $CsPbX_3$ NCs: ODE (5 mL) and PbX_2 (0.188 mmol) such as PbI_2 (0.087g, ABCR, 99.999%), $PbBr_2$ (0.069g, ABCR, 98%), $PbCl_2$ (0.052g, ABCR, 99.999%) or their mixtures were loaded into 25 mL 3-neck flask and dried under vacuum for 1h at 120 ºC. Dried oleylamine (0.5

mL, OLA, Acros 80-90%) and dried OA (0.5 mL) were injected at 120 ºC under N_2. After complete solubilisation of a PbX_2 salt, the temperature was raised to 140-200 ºC (for tuning the NC size) and Cs-oleate solution (0.4 mL, 0.125 M in ODE, prepared as described above) was quickly injected and, 5s later, the reaction mixture was cooled by the ice-water bath. For $CsPbCl_3$, higher temperature of 150 ºC and 1 mL of trioctylphosphine (TOP, Strem, 97%) are required to solubilize $PbCl_2$.

Isolation and purification of $CsPbX_3$ NCs. The crude solution was cooled down with water bath and aggregated NCs were separated by centrifuging. For smaller NCs synthesized below 160 ºC, centrifugation at 0 ºC or addition of tert-butanol (^{t}BuOH, Merck, 99%) to the crude solution (ODE:^{t}BuOH=1:1 by volume) were found to be helpful for a complete precipitation. After centrifugation, the supernatant was discarded and the particles were redispersed in toluene or hexane forming long-term colloidally stable solutions.

Photo-polymerization reaction: First, a photoinitiator (10 mg, Irgacure 819, a gift from Prof. H. Grützmacher, also commercially available BASF) was dispersed in methyl methacrylate (1 mL, MMA, Aldrich, 99%). Then a NCs/hexane solution (120 µL, concentration of $CsPbX_3$ NCs of *ca.* 20 mg/mL) was added to MMA/photoinitiator mixture. After drying the hexane, the mixture was placed into an arbitrary shaped container (NMR tube, Petri dish *etc.*). The polymerization took place under UV irradiation for 1h or under daylight for 12-24h (in a glovebox, to avoid oxygen during the polymerization).

Characterization Methods

Absorbance: UV-Vis absorption spectra for colloidal solutions were collected using a Jasco V670 spectrometer in transmission mode.

Photoluminescence (PL) and absolute quantum yield (QY) measurements. Fluorolog iHR 320 Horiba Jobin Yvon spectrofluorimeter equipped with a PMT detector was used to acquire steady- state PL spectra from solutions and films. PL QYs were estimated according to standard procedure using appropriate dye molecules for blue, green and red spectral regions (coumarine 343, fluorescein, and rhodamine 6G).[1]

In-situ photoluminescence measurements were performed with excitation light from CW laser (405 nm) delivered through one branch of Y-shaped fiber optic bundle to the flask during synthesis, and collecting the PL with the second branch. PL was dispersed with Acton Research

SpectraPro MS2300i monochromator (600 groves/mm grating) and recorded with Thorlabs LC100/M CCD line array detector with a speed of 100 spectra/second.

Time-resolved PL measurements. PL lifetime measurements were performed using a time-correlated single photon counting setup (TCSPC) utilizing SPC-130-EM counting module and BDL-488-SMN picosecond laser (Becker & Hickl), as an excitation source, with pulse duration of 50 ps, wavelength of 488 nm and CW power equivalent of about 0.5 mW. The laser was externally triggered with periods of 50-1000 ns by pulse generator HP 8116A. IDQ-ID-100-20-ULN avalanche photodiode (Quantique) was used to record the decay traces.

Powder X-ray diffraction patterns (XRD) were collected with STOE STADI P powder diffractometer, operating in transmission mode. Germanium monochromator, Cu Kα1 irradiation and silicon strip detector Dectris Mythen were used.

Transmission electron microscopy (TEM) images were recorded using JEOL JEM-2200FS microscope operated at 200kV.

Energy dispersive X-ray (EDX) spectroscopy. Elemental analysis was performed with two scanning electron microscopes (Zeiss Gemini 1530 and Hitachi S-4800).

Rutherford backscattering spectrometry (RBS) was performed at the ETH Laboratory of Ion Beam Physics. Measurements were conducted using a 2 MeV 4He beam and a silicon PIN diode detector under angle of 168°. The collected RBS data was analyzed using simulations by the RUMP code.[2]

Computational Methods

Total energy calculations for polymorphs of $CsPbX_3$ (X=Br, I). The cubic and the orthorhombic structures of $CsPbBr_3$ and $CsPbI_3$ were optimized using the CASTEP code, with the generalized gradient form (GGA) of the exchange-correlation functional (Perdew-Burke-Ernzerhof96, PBE) and norm-conserving pseudo-potentials. The Brillouin zone were sampled by using a fine mesh commensurate to the specific lattice dimensions, but with the actual spacing below 0.025 $Å^{-1}$. The energy threshold, the maximum atomic displacement, the maximum atomic force and the lattice stress were set to 0.001 meV/atom, 0.0005 Å, 0.001 eV/ Å and 0.002 GPa, respectively.

Electronic structure calculations for cubic $CsPbX_3$ (X=Cl, Br, I). The electronic structure of the cubic phases of $CsPbX_3$ (X = Cl, Br, I) were calculated using density functional theory, including scalar relativistic and spin-orbit interactions in the code VASP.[3-4] Initial structure relaxation was performed at the level of the semi-local PBEsol functional,[5] which was augmented with non-local PBE0 calculations including 35% Hartree-Fock exchange for a more quantitative description of the electronic structure. A plane-wave cutoff of 500 eV and a *k*-point grid density of 6×6×6 was employed throughout.

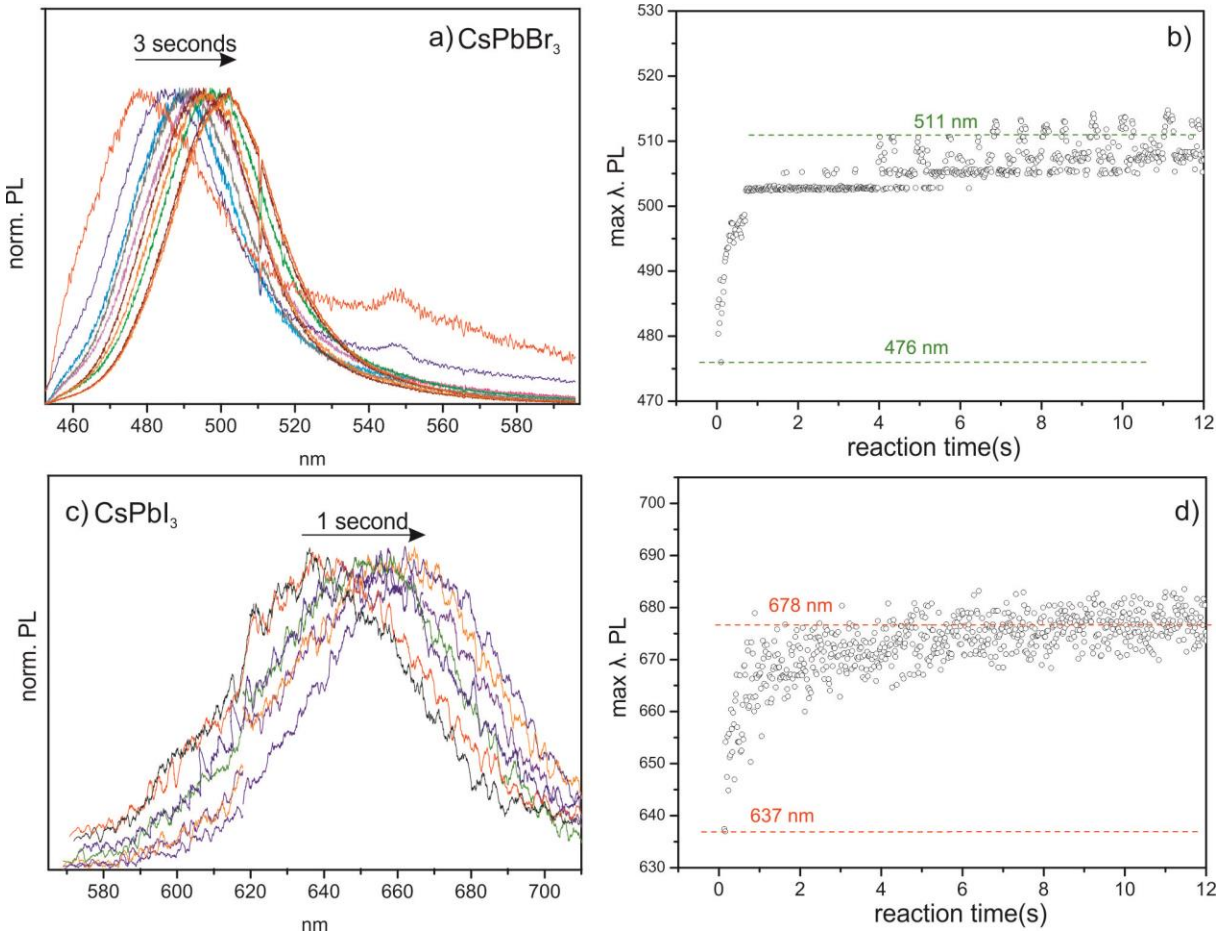

Figure S1. In-situ PL study during the formation of $CsPbBr_3$ and $CsPbI_3$ NCs. (a, c) Selected PL spectra showing the evolution of PL peak and spectral linewidth. (b, d) Detailed kinetics of the PL peak evolution. Data points were taken with 10 ms intervals.

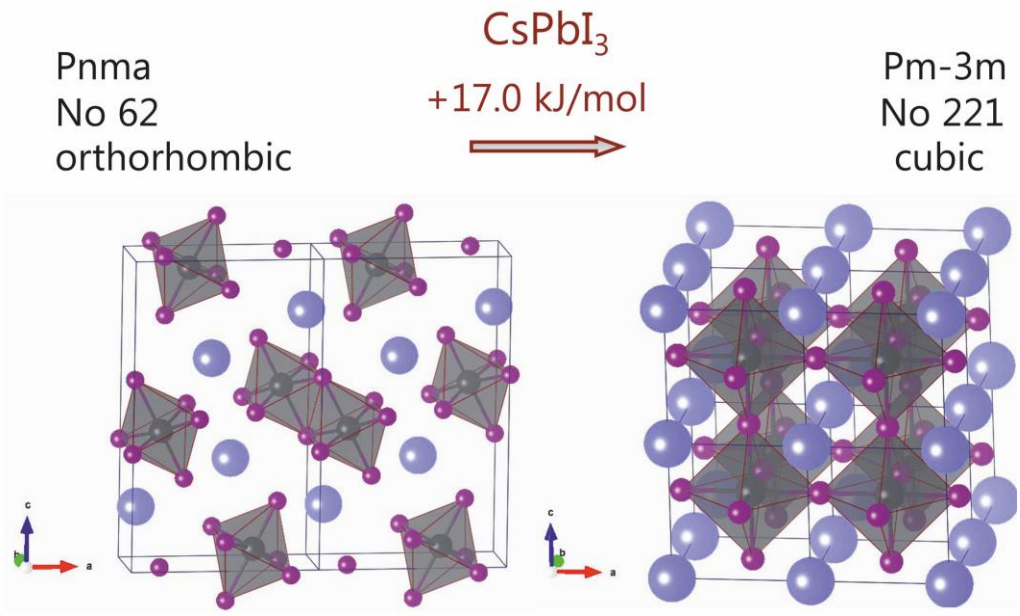

Figure S2. The orthorhombic and cubic structures of $CsPbI_3$. The perfect corner-sharing octahedra of $[PbI_6]$ in the cubic structure become distorted (distortion index of 0.0176 in bond lengths) and edge-sharing in the orthorhombic structure. Representing colors: Cs (violet); Pb (grey), I (purple).

Table S1. The structural data for the orthorhombic and cubic structures of $CsPbI_3$ (GGA-DFT, CASTEP).

Space group	species	○ *x*	○ *y*	○ *z*	site	symmetry
Pnma (62) a = 10.028 Å b = 4.853 Å c = 18.164 Å	Cs	0.4280	0.6739	0.25	4c	.m.
	Pb	0.1637	0.25	0.4411	4c	.m.
	I	0.1668	0.25	0.0029	4c	.m.
	I	0.0214	0.25	0.6067	4c	.m.
	I	0.2894	0.25	0.2888	4c	.m.
Pm-3m (221) a = 6.348 Å	Cs	0.5	0.5	0.5	1b	m-3m
	Pb	0	0	0	1a	m-3m
	I	0.5	0.5	0.5	3d	4/mm.m

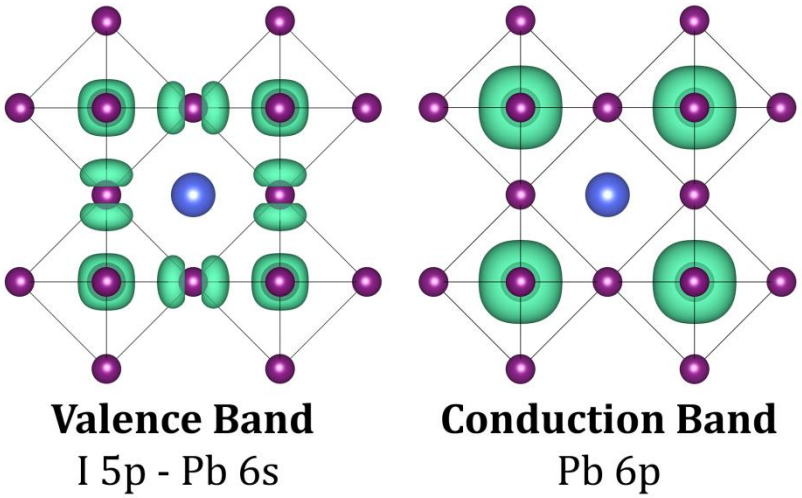

Figure S3. The calculated electron density associated with the upper valence band and lower conduction band of cubic $CsPbI_3$. Note both hole and electron states will be associated with the PbI_3 framework, supporting carrier transport in three dimensions. Similar electron distributions are found for the chloride and bromide systems. The frontier electronic structure is determined by the PbX_3 framework, with both hole and electron density distributed on the corner-sharing octahedral framework, which is similar to the hybrid halide perovskite $CH_3NH_3PbI_3$.[6-7] The changes in the band gap observed for each material are primarily driven by the valence orbitals of the halide ion, where the atomic orbitals increase in binding energy from I (5p) to Br (4p) to Cl (3p), while the Pb 6p orbitals that form the conduction band remain relatively unperturbed.

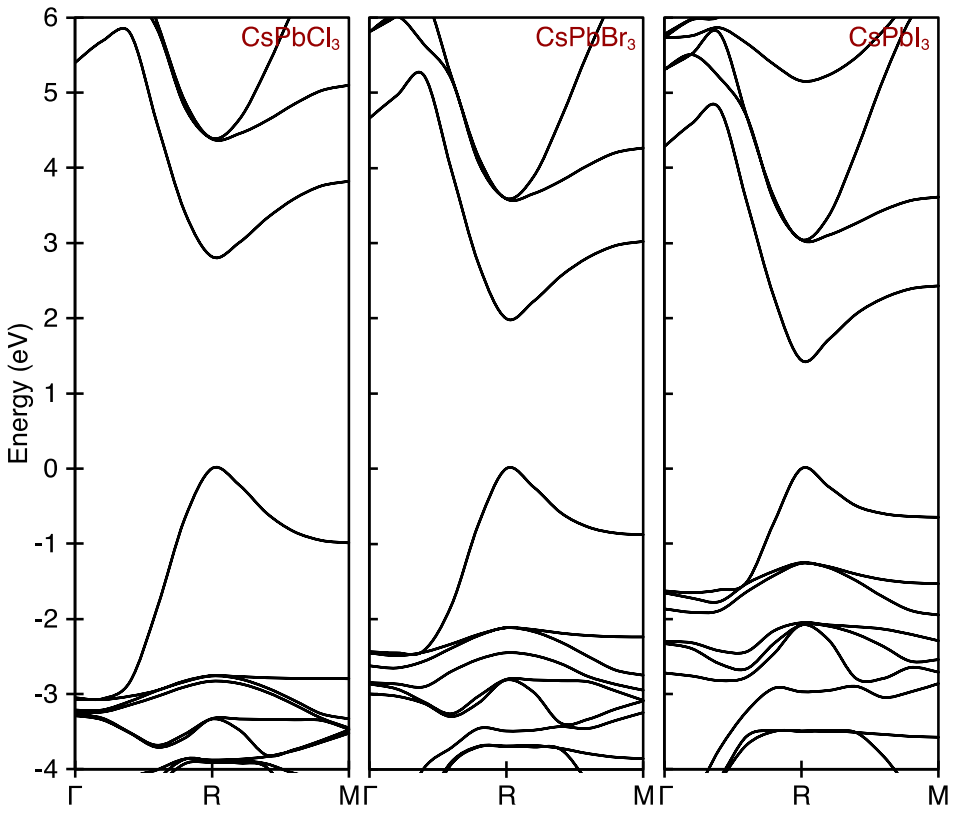

Figure S4. The calculated electronic band structures for the three cesium lead halide perovskites (cubic phase), including relativistic corrections, from density functional theory (VASP code). The top of the valence band is set to 0 eV in each case. Note the similar dispersion relations in the valence and conduction bands, which are plotted from G (0,0,0) to R (½,½,½) to M (½,½,0) in the first Brillouin zone. From the electronic band dispersion (Figure S4), the effective masses of the electrons and holes were determined (within k_BT of the band edges). The high frequency dielectric constants were calculated using density functional perturbation theory.[8] A range of electronic properties for each material is summarized in Table S2.

Table S2. The calculated properties of the three ternary halides (cubic phase) from density functional theory (VASP code), including the effective carrier masses and the high-frequency optical dielectric constants. The values are predicted at the equilibrium lattice constant and temperature effects are not included. There is a constant offset in the band gaps of ~0.2 eV with respect to the room temperature experimental values. The average hole and electron effective are given in units of electron mass.

	E_g (eV)	m_h^*	m_e^*	ε^∞
$CsPbCl_3$	2.82	0.17	0.20	4.07
$CsPbBr_3$	2.00	0.14	0.15	4.96
$CsPbI_3$	1.44	0.13	0.11	6.32

Within effective mass theory,[9] the effective Bohr diameter of a Wannier-Mott exciton can be defined from:

$$a_0 = \frac{2\hbar^2\varepsilon^\infty}{m^* e^2}$$

where ε^∞ represents the effective dielectric constant and m^* is the reduced carrier mass. The corresponding binding energy between electrons and holes is:

$$E_b = \frac{2\hbar^2}{m^* {a_0}^2}$$

The values for each material are summarised in Table S2. Furthermore, from these values the extend of quantum confinement in a spherical potential well of radius *r* can be estimated from

$$\Delta E = \frac{\hbar^2\pi^2}{2m^* r^2}$$

which has been used to calculate the size dependence of the quantum confinement of the $CsPbBr_3$.

Table S3. The calculated optical Mott-Wannier exciton properties (binding energy in meV and diameter in nm) of the three halide perovskites (cubic phase) from effective mass theory using the values reported in Table S1. Values are shown for the limit of the high frequency optical dielectric constant.

	E_b (meV)	a_0 (nm)
$CsPbCl_3$	75	5
$CsPbBr_3$	40	7
$CsPbI_3$	20	12

Supporting References

(1) Grabolle, M.; Spieles, M.; Lesnyak, V.; Gaponik, N.; Eychmüller, A.; Resch-Genger, U. *Anal. Chem.* **2009**, *81*, 6285-6294.

(2) Doolittle, L. R. Nucl. Instr. and Meth. B **1986**, *15*, 227-231

(3) Kresse, G.; Joubert, D. *Phys. Rev. B* **1999**, *59*, 1758.

(4) Kresse, G.; Furthmüller, J. *Phys. Rev. B* **1996**, *54*, 11169.

(5) Perdew, J. P.; Ruzsinszky, A.; Csonka, G. I.; Vydrov, O. A.; Scuseria, G. E.; Constantin, L. A.; Zhou, X.; Burke, K. *Phys. Rev. Lett.* **2008**, *100*, 136406.

(6) Frost, J. M.; Butler, K. T.; Brivio, F.; Hendon, C. H.; van Schilfgaarde, M.; Walsh, A. *Nano Lett.* **2014**, *14*, 2584-2590.

(7) Brivio, F.; Butler, K. T.; Walsh, A.; van Schilfgaarde, M. *Phys. Rev. B* **2014**, *89*, 155204.

(8) Baroni, S.; de Gironcoli, S.; Dal Corso, A.; Giannozzi, P. *Rev. Mod. Phys.* **2001**, *73*, 515.

(9) Yu, P. Y.; Cardona, M. *Fundamentals of semiconductors*; Springer, 1996.